Journal of the Ceramic Society of Japan **114** [11] 937–949 (2006)

Paper

Thermodynamic Assessment of the PZT System

Marija CANCAREVIC*,**, Matvei ZINKEVICH* and Fritz ALDINGER*

*Max-Planck Institut für Metallforschung und Institut für Nichtmetallische Anorganische Materialien der Universitat Stuttgart, Heisenbergstr., Stuttgart, Germany

**Institute of Nuclear Science "Vinca", Department of Material Science, Belgrad, Serbia

The thermodynamic assessment of the PZT system is carried out by the CALPHAD method. The thermodynamic properties of the phases are described using compound energy formalism (CEF) for the various solid phases and a solution model for the liquid. Three boundary systems PbO–ZrO_2, PbO–TiO_2 and ZrO_2–TiO_2 are reassessed based on the most recent experimental data, while the ternary PbO–TiO_2–ZrO_2 system is modelled for the first time. Calculated phase diagrams are compared with the experimental data.

[Received July 11, 2006; Accepted September 21, 2006]

Key-words : *PZT, Phase diagram, Thermodynamics, CALPHAD*

1. Introduction

$PbZr_xTi_{1-x}O_3$ (PZT) or modified PZT solid solutions are of interest for many years for technological applications, which result from their piezoelectric, ferroelectric and pyroelectric properties. Although extensive experimental studies of the PZT system have been carried out in the past attention was paid mainly to physical properties, kinetics and device characterisation, while a little to phase equilibria and thermodynamic considerations. Knowledge of phase equilibria and thermodynamics of the quaternary O–Pb–Ti–Zr system is important for the optimization of manufacturing and sintering conditions of the PZT ceramics as well as for tailoring their physical properties.

A review of the literature data on the O–Pb–Zr system has been presented by Cancarevic et al..[1] Experimental studies of the O–Pb–Zr and O–Pb–Ti systems are confined to the investigation of lead zirconate and lead titanate, and the quasi-binary systems (PbO–ZrO_2 and PbO–TiO_2). The modelling of quasibinary PbO–ZrO_2 and PbO–TiO_2 systems was done by Koo et al.[2] and Soh et al.,[3] respectively. Thermodynamic assessments of ZrO_2–TiO_2 system were published by several authors.[4)–6)] However, they differ markedly from each other. Thermodynamic modelling of the quasiternary PbO–ZrO_2–TiO_2 system has not been done so far.

It is easy to accept that the combination of thermodynamics and visualized phase diagrams can be an efficient tool to described and analyze the phase equilibria and phase transformations under both, equilibrium and non-equilibrium conditions. The CALPHAD (CALculation of PHAse Diagrams) approach[7),8)] is a method to assess thermodynamic parameters using the diverse type of experimental information: phase diagrams, calorimetry, vapor pressure data, electrochemical measurements, etc. The optimal values of the unknown parameters providing the best match between calculated quantities and their experimental counterparts are usually obtained by the weighted non-linear last squares minimization or fitting procedure (thermodynamic optimization). The selection of the model for a phase must be based on its physical and chemical properties of such as crystallographic structure, type of bonding, ordering, and defect structure. The CALPHAD method is implemented in several commercial software packages based on the different mathematical methods and computer languages (Thermo-Calc, Pandat, MTDATA, Fact Sage...) In the present work, all computations were done using Thermo-Calc software package.[9] Thermo-Calc is general and flexible software for the thermodynamic properties and phase diagram calculations based on the minimization of Gibbs energy of the system. Thermo-Calc is for example the only software that allows explicit condition of individual phase compositions or configuration whereas most software can handle condition on the overall composition only. Thermo-Calc software consists of several basis modules, i.e., TDB for database retrieval and management, TAB for thermodynamic property tabulation of phases and reactions, POLY3 for calculations of individual equilibria and phase diagrams, PARROT for parameter optimizations, etc.

The purpose of this work is to revise three boundary systems using the most recent experimental information to obtain a self-consistent thermodynamic description of the PbO–ZrO_2–TiO_2 system based on the available data on phase equilibria and thermodynamic properties.

2. Survey of the literature information

2.1 PbO–ZrO_2

Literature information mainly belongs to investigations of the crystallographic and dielectric properties of the lead zirconate with only few phase diagram and thermodynamic studies. Three stable perovskite-type phases have been found at the $PbZrO_3$ composition: the orthorhombic low-temperature (α,[10] up to 504 K) phase is antiferroelectric, the intermediate (γ,[11] from 504 to 507 K) is ferroelectric and cubic high-temperature (β,[12] up to the melting point $T_m = 1843$ K) phase is paraelectric (**Table 1**). The paraelectric→ferroelectric→antiferroelectric phase transition temperatures depend on the oxygen nonstoichiometry and on the compositional deviations caused by the sublimation of PbO.[13] Until now, the basic structure parameters have mainly been investigated for the antiferroelectric phase. The questions regarding the existence of polarization and the true crystal structure of lead zirconate are still open. The crystallographic data for lead oxides[14),15)] and zirconia[16),17)] are also shown in Table 1.

Quasibinary section of the PbO–ZrO_2 system was published by Fushimi and Ikeda.[18] Cubic $PbZrO_3$ decomposes to tetragonal ZrO_2 and a liquid phase containing ~90 mol.% PbO at 1843 K.[18] A few investigations have been performed in the PbO-rich part of the PbO–ZrO_2 system[18)–20)] but results are contradictory. Harris[20] reported that X-ray analysis of the samples $PbO + ZrO_2$ in 1 : 1 molar ratio heated to 1563 K indicated the presence of $\beta PbZrO_3$, monoclinic ZrO_2, and tetragonal PbO. The latter had a tetragonal structure rather than the orthorhombic structure of yellow βPbO. This finding

Table 1. Solid Phases

Phase, temp. range (K)	Pearson symbol/ Space Group/ Prototype	Lattice parameters (pm) and angles	Comments/Reference
α $PbZr_xTi_{1-x}O_3$ T< 504 x > 0.9	*oP*40 *Pbam* –	*a* = 588.194; *b* =1178.206; *c* = 822.946	pure $PbZrO_3$ at 298 K [10]
γ $PbZrO_3$ 504 < T < 507	*cF** *F2mm* –	–	[11]
β $PbZr_xTi_{1-x}O_3$ 507 < T < 1843	*cF** *Fm-3m* –	*a* = 415 *a* = 414.49	pure $PbZrO_3$ [12] $PbZr_{.9}Ti_{.1}O_3$ [66]
α PbO *T* < 760	*tP*4 *P4/nmm* PbO	*a* = *b* = 397.44; *c* = 502.20	mineral name: litharge [14]
β PbO *T* > 760	*oP*8 *Pbcm* PbO	*a* = 589.31; *b* = 549.04; *c* = 475.28;	mineral name: massicot [15]
α ZrO_2 *T* < 1478	*mP*12 *P*2_1/*c* –	*a* = 515.104; *b* = 520.31; *c* = 531.514; β = 99.197°	mineral name: baddeleyite [16]
β ZrO_2 1478 < *T* < 2650	*tP*6 *P*4_2/*nmc* HgI_2	*a* = *b* = 359.482; *c* = 518.247;	[17]
γ ZrO_2 *T* > 2650	*cF*12 *Fm*3*m* CaF_2	*a* = 494.72	[17]
α′ $PbZr_xTi_{1-x}O_3$ *T< 763 x < ~ 0.5	*tP*5 *P4mm* –	**a* =**b* = 390.231 * *c* = 403.292 ***a* =* **b* = 395.251 ** *c* = 414.84	* pure $PbTiO_3$ at 298 [32] * *$PbZr_{.2}Ti_{.8}O_3$ [67]
TiO_2 Rutile	*tP*6 *P*4_2/*mnm* Rutile	*a* = *b* = 459.37; *c* = 295.87	[34]
(I) TiO_2 Anatase	*tI*12 *I*4_1/*amd* –	*a* = *b* = 378.216; *c* = 950.226	metastable [35]
(II) TiO_2 Brookite	*oP*24 Pbca –	*a* = 917.42; *b* = 544.92; *c* = 513.82;	metastable [36]
$PbTi_3O_7$ T < 813	*mP*22 *P*1$2_1$/*m*$_1$ –	*a* = 1071.85; *b* = 381.21; *c* = 657.77; β = 98.277°	at 298 K [37]
β $Zr_xTi_{1-x}O_4$ 1443 < T < 2103 0.41 < x <0.59	*oP*12 *Pbcn* αPbO_2	*a* = 480.422; *b* = 548.253; *c* = 503.132	mineral name: Srilankite [46]
α' $ZrTiO_4$ ($ZrTi_2O_6$, $Zr_5Ti_7O_{24}$) T < 1343	*oP*36 *Pbcn* –	*a* = 1435.74; *b* = 532.47; *c* = 502.00	[46]
α $ZrTiO_4$ 1343 < T < 1443	– *Pbcn* –	*a* = 960; *b* = 530; *c* = 500	[47],[48]
γ' $PbZr_xTi_{1-x}O_3$ ~ 0.6 < x < ~ 0.95 T < ~ 423	*hR*10 $R\bar{3}c$ –	*a* = *b* = 585.64 *c* = 1439.51 β =120°	$PbZr_{.9}Ti_{.1}O_3$ [66]
δ $PbZr_xTi_{1-x}O_3$ x > 0.5 T < ~ 660	*hR*5 $R\bar{3}m$ –	*a* = *b* = *c* = 410.01 α = β = γ =89.73°	$PbZr_{.75}Ti_{.25}O_3$ [68]
ε $PbZr_xTi_{1-x}O_3$ 0.50 < x < 0.52	*mS*10 C_1m_1 –	*a* = 570.82; *b* = 570.78; *c* = 414.14; β = 90.199°	$PbZr_{.52}Ti_{.48}O_3$ [72]

was confirmed by Jacob and Shim[19] by heating an equimolar mixture of βPbO and αZrO_2 up to 1228 K, followed by cooling in air and X-ray analysis. This observation is not in accord with the phase diagram of Fushimi and Ikeda,[18] but consistent with the assessed phase diagram.[2] A detailed study of the PbO-rich side of the PbO–ZrO_2 phase diagram is required to check the temperature and composition of the various phase fields.

Thermodynamic properties of $PbZrO_3$ were investigated by several groups.[19),21)–26] The experimental investigations were mainly performed on the high-temperature cubic modification, $\alpha PbZrO_3$, except the study of[21] on the low-temperature orthorhombic, αPbZrO$_3$, modification. Onodera et al.[22] measured the heat capacity of single crystals of antiferroelectric αPbZrO$_3$ in a wide temperature region (from room temperature to 650 K) by AC calorimetry, but has drawn the curve in arbitrary units. Heat capacity curve showed a sharp change at 504.5 K, due to transformation into the high temperature modification βPbZrO$_3$. The transition entropy was reported to be $\Delta S = 1.65\ \mathrm{J \cdot mol^{-1} \cdot K^{-1}}$. Gospodinov and Marchev[21] reported the thermodynamic functions (C_p, S, $H_T - H_{298}$) of the low-temperature orthorhombic modification (α) from room temperature to 504 K. The low-temperature heat capacity data of αPbZrO$_3$ are missing, while the results of Gospodinov and Marchev[21] are not in agreement with the PbO–ZrO$_2$ phase diagram reported by Fushimi and Ikeda.[18] The Gibbs energy of formation of lead zirconate calculated from earlier vapor pressure studies (assuming that the vapor phase consists entirely of monomeric PbO molecules)[23)–25] is inconsistent with the EMF (electromotive force) measurements reported by Jacob and Shim[19] and the calculated PbO–ZrO$_2$ quasibinary phase diagram, which suggests decomposition of lead zirconate to tetragonal ZrO$_2$ and a liquid phase containing ~90 mol.% PbO at 1843 K. Since the vapor phase over pure solid and liquid PbO consist of polymeric species of type Pb$_n$O$_n$ ($1 \le n \le 6$) results based on the vapor pressure measurements differ significantly from those obtained by EMF measurements.[19] At the same time, most recent data from the vapor pressure measurement reported by Popovic et al.[26] (existence of PbO$^+$ and Pb$_2$O^{2+} ions was experimentally detected) show good agreement with results of Jacob and Shim.[19] Recently, the enthalpy of formation of PbZrO$_3$ was measured by drop solution calorimetry.[27] The heat content and entropy of βPbZrO$_3$ are not known, while thermodynamic data for the other phases (liquid, PbO solid solutions) are completely missing.

2.2 PbO–TiO$_2$

The experimental phase diagram of this system has been reported by several authors.[28,29] However, there is no agreement about the existence of intermediate compounds and their homogeneity ranges. The equilibrium phases in the PbO–TiO$_2$ system are PbO solid solution (tetragonal and orthorhombic), liquid, rutile and PbTiO$_3$ with a perovskite-type structure, while the existence of Pb$_2$TiO$_4$ and Pb$_2$Ti$_2$O$_8$ is doubtful. Only one intermediate compound, PbTiO$_3$, was reported in the PbO–TiO$_2$ quasi-binary system by Rase et al.,[28] while the previously reported Pb$_2$TiO$_4$[30,31] was not observed. PbTiO$_3$ exists in two polymorphic forms, tetragonal (α',[32] up to 763 K) and cubic (β, 763–1558 K) (Table 1). The ternary PbTi$_3$O$_7$ compound was found in the TiO$_2$-rich side[29,33] and it was included in the isobaric section PbO$_x$–TiO$_2$ in air.[29] The upper limit of stability of PbTi$_3$O$_7$ was supposed to be 813 K as confirmed by X-ray diffraction results. The crystallographic data for TiO$_2$[34–36] and PbTi$_3$O$_7$[37] are also listed in Table 1.

Thermodynamic properties of PbTiO$_3$ were investigated by several groups.[23–27,38–40] The enthalpy of formation of PbTiO$_3$ using the drop solution calorimetry was measured by Rane and Navrotsky,[27] while the Mehrotra et al.[38] as well as Shim and Jacob[39] measured the free energy of formation. The specific heat of pure lead titanate (PbTiO$_3$) in the temperature range from 325 to 1250 K was studied by Rossetti and Maffei.[40] Vapour pressure measurements using the Knudsen technique were done by many authors.[23–26] Results of Schmal et al.,[23] Haerdtl and Rau[24] and Holman and Fulrath[25] are in a good agreement, while the data reported by Popovic et al.[26] shows significant deviations.

Soh et al.[3] published the thermodynamic calculation of the PbO–TiO$_2$ system using a quasi-regular model to express the Gibbs energy of all solution phases. The Gibbs energy of PbTiO$_3$ compound was evaluated on the base of estimated thermodynamic properties (heat capacity) compiled by Barin.[41]

2.3 ZrO$_2$–TiO$_2$

The solid solutions with Zr : Ti molar ratio ranging from 1 : 1 to 1 : 2 are the only stable compounds in the ZrO$_2$–TiO$_2$ system. Two structural modifications are known: high temperature disordered and low temperature ordered phase[42–48] (Table 1). Two types of ordered structures with different stoichiometries were reported by Park et al..[49] ZrTiO$_4$ is known to undergo a successive ordering transition between 1400 and 1100 K.[49,50] Above 1400 K it crystallizes in an orthorhombic αPbO$_2$ type structure, with the random distribution of Zr and Ti over the octahedral site[46,51] (Table 1). Slow cooling of the disordered polymorph below 1400 K results in distinct shortening of the crystallographic b-axis, which is due to increasing order of Zr and Ti, as evident by the formation of superstructure reflections.[49] Park et al.[49] suggested that the ordering transition occurs in several steps from the normal phase (disordered βZr$_{1-x}$Ti$_x$O$_4$, T > 1400 K) via an incommensurate state (partially ordered αZrTiO$_4$, $1400 > T > 1100$ K) to the commensurate phase (ordered α'ZrTiO$_4$,). The fully ordered phase α'ZrTiO$_4$ has composition close to ZrTi$_2$O$_6$[43] but the same structure also occurs for Zr$_5$Ti$_7$O$_{24}$.[46]

The ZrO$_2$–TiO$_2$ phase diagram has been studied intensively over many years.[43,44,50,52–61] However, no general agreement among the proposed phase diagrams exists. While detailed phase diagrams are available for the high temperature regions above 1473 K,[50,56,59] where reactions proceed rapidly, the low temperature phase relations are not well established. Experimental studies disagree significantly on the location of the two phase field tetragonal-monoclinic ZrO$_2$ solid solutions[53,55,57,58,61] because heating and cooling experiments are characterised by a hysteresis effect. Another problem is caused by sluggish kinetics and difficulty in performing experiments at relatively low temperatures (< 1473 K). Discrepancies are mainly concerned with the existence of intermediate compounds and its homogeneity range. Three intermediate compounds were reported by Troitzsch et al.[61] and McHale et al.,[43] while earlier studies indicated the absence of any compounds in the system and the presence of partial solid solutions.[52,58,62] Both, McHale and Roth[43] and Troitzsch et al.[44,61] reported the existence of the disordered high-temperature βZr$_{1-x}$Ti$_x$O$_4$ phase with a wide homogeneity range, while its stability range and adjacent phase field with the ordered low-temperature phases αZrTiO$_4$ and ZrTi$_2$O$_6$ differ significantly. The low-temperature technique of solid solution formation via coprecipitation from alkoxides solution was used as an alternative method of preparation for a wider range of compositions in the system ZrO$_2$–TiO$_2$,[43] to enable determination of the low-temperature solid solution region and structure without the influence of prior high-temperature heat treatment. Although, there is an agreement between different authors[43,61] about the existence of intermediate compounds and solid solution of the end-members (titania, monoclinic and tetragonal zirconia), the solubility ranges markedly differ, particularly in the ZrO$_2$-rich range, close to monoclinic-tetragonal transformation. In addition, experimental data on the homogeneity range of the cubic zirconia are missing and it has been drawn tentatively.[53,57,59,60] Liquidus and solidus were studied by Shevchenko et al.,[59] Coughanour et al.[50] and Noguchi and

Mizuno.[56] Liquidus of the system has two inflections, which correspond to 35 and 60 mole% TiO_2,[59] and eutectic point at 73 mole% and 1993 K[59] or 80 mole% TiO_2 and 2033 K.[50] High temperature $\beta ZrTiO_4$ phase melts incongruently at 2093[50] or 2103 K.[59]

The thermodynamic data of formation and molar heat capacity from 5 to 380 K of $ZrTiO_4$ compound were measured by Hom et al..[63] No other works concerning the thermodynamics of the phases in this system are available.

2.4 PbO–ZrO_2–TiO_2 system

The perovskite-structured ferroelectrics in the $Pb(Zr_xTi_{1-x})O_3$ (PZT) system provide an unusual example of a complete solid solution between the end-members compounds $PbTiO_3$ and $PbZrO_3$.[25),26),28),55),64] At high temperatures, $Pb(Zr_xTi_{1-x})O_3$ crystallises as disordered substitutional solid solutions to a cubic perovskite prototype phase of symmetry *Pm*3*m* for all values of *x*. Intermediate solid solutions compositions with different Zr/Ti ratio adopt orthorhombic, tetragonal and rhombohedral symmetries at temperatures between 273 and 763 K due to a variety of cation shifts, octahedral tilts and deformations[65)–68] (Table 1). Recent literature data indicate also the existence of monoclinic modification at low temperatures.[69)–72] At room temperature these include the lower-symmetry antiferroelectric, orthorhombic structure ($\alpha PbZr_xTi_{1-x}O_3$ phase) of $PbZrO_3$.[73] All its solid solutions with more than 10 mol% of $PbTiO_3$ are ferroelectric. With increasing Ti content, two ferroelectric rhombohedral phases are observed up to around $x \approx 0.5$ where there is transition into a ferroelectric tetragonal phase ($\alpha' PbZr_xTi_{1-x}O_3$) continuing to the end member $PbTiO_3$.[66] At room temperature, the rhombohedral low-temperature phase ($\gamma' PbZr_xTi_{1-x}O_3$) has space group $R\bar{3}c$ and exhibits both cation shifts and octahedral tilting.[74] As temperature increase the octahedral tilts are known to disappear[66] leading to the phase transformation to high temperature rhombohedral phase ($\delta PbZr_xTi_{1-x}O_3$) and space group $R\bar{3}m$. A further increase in temperature diminishes the cation shifts until the final phase transition into the cubic perovskite structure ($\beta PbZr_xTi_{1-x}O_3$ phase) occurs. Monoclinic-tetragonal phase transition was observed at low temperature in $PbZr_xTi_{1-x}O_3$ solid solutions in the vicinity of the morphotropic phase boundary (MPB) ($x=0.5$–0.55).[69),70),72),75)–77]

The experimental phase diagram of the PZT system at higher temperatures was investigated by few groups[18),55),64] (**Table 2**), while there were many studies concerning the low temperature phase relations.[65),75)–83] Webster et al.[55] published the isothermal section at 1373 K for the titania and zirconia rich part of ZrO_2–TiO_2–PbO system (ZrO_2–TiO_2–$PbTiO_3$–$PbZrO_3$), while the isothermal sections at 1373, 1473 and 1573 K of the PbO-rich part of the system were studied by Fushimi and Ikeda.[18] Pseudobinary section $PbZrO_3$–$PbTiO_3$ was reported by Fushimi and Ikeda[18] and Moon et al..[64] Temperature of peritectic reaction, $L+\beta ZrO_2$ (tetragonal)$\rightarrow \beta PbZr_xTi_{1-x}O_3$ ($x \sim 0.4$), was found to be 1613[18] or 1633 K,[64] while somewhat lower solidus and liquidus temperatures were measured in.[64] Results of these studies are in satisfactory agreement and differences are within the uncertainty of measurements. Work of Holman et al.[25] was mainly concerned with the width of the homogeneity range of $\beta Pb_{1-y}\square_y(Zr_xTi_{1-x})O_{3-y}$ solid solutions at 1373 K.

Thermodynamics properties of the $\beta PbZr_xTi_{1-x}O_3$ solid solutions are mainly derived from the PbO–vapor pressure measurements using the Knudsen technique.[23)–26] Rane et al.[27] reported the standard enthalpies and heat of mixing in the cubic lead zirconate titanate solid solutions using drop solution calorimetry (**Table 3**).

3. Thermodynamic modelling

Gibbs energy functions of the end members PbO and ZrO_2 are adopted from the assessments of the corresponding binary systems,[84),85] while the thermodynamic properties of TiO_2 are evaluated by Cancarevic et al..[86] The Gibbs energy functions of the stoichiometric solid phases and end-members of solutions are given by

$$^{\circ}G(T)=G(T)-H^{SER}=a+bT+cT\ln(T)+dT^2+eT^3+f/T+\sum_n g_nT^n \quad (1)$$

where H^{SER} is the molar enthalpy of the stable element reference (SER) at 298.15 K, *a* to *f* and g_n are coefficients and *n* stands for a set of integers. The stoichiometric compounds $PbTiO_3$, $PbZrO_3$, $\alpha ZrTiO_4$ and $ZrTi_2O_6$ ($\alpha' ZrTiO_4$) are represented by the formula $(Pb^{2+})_1(Ti^{4+})_1(O^{2-})_3$, $(Pb^{2+})_1(Zr^{4+})_1(O^{2-})_3$, $(Zr^{4+})_1(Ti^{4+})_1(O^{2-})_4$ and $(Zr^{4+})_1(Ti^{4+})_2(O^{2-})_6$, respectively. The heat capacity of $ZrTi_2O_6$, $\alpha ZrTiO_4$ and $PbZrO_3$ compounds is described by using Neumann–Kopp rule, i.e. as an average of the heat capacities of PbO, TiO_2 and ZrO_2.

The gas phase is described as an ideal mixture containing the species Ti, TiO, TiO_2, O, Zr, Zr2, ZrO_2, O_2, O_3, Pb, Pb_2, PbO, Pb_2O_2, Pb_3O_3, Pb_4O_4, Pb_5O_5, and Pb_6O_6. The Gibbs energy of the gas phase is given as

$$G^{gas}=\sum_i x_i {^{\circ}G_i^{gas}}+RT\sum_i x_i\ln x_i+RT\ln\frac{P}{P_0}, \quad (2)$$

where x_i is the mole fraction of the specie *i* in the gas phase, $^{\circ}G_i^{gas}$ is the standard Gibbs energy of the gaseous specie *i*,[84),87] *R* is the gas constant, and P_0 is the standard pressure of 1 bar.

The Gibbs energy of the liquid and PbO solid solution is described by substitutional solution model (PbO, TiO_2, ZrO_2) as

$$G^{\varphi}=x_{PbO}\cdot{^{\circ}G^{\varphi}_{PbO}}+x_{TiO_2}\cdot{^{\circ}G^{\varphi}_{TiO_2}}+x_{ZrO_2}\cdot{^{\circ}G^{\varphi}_{ZrO_2}}+R\cdot T(x_{PbO}\cdot\ln x_{PbO}+x_{TiO_2}\cdot\ln x_{TiO_2}+x_{ZrO_2}\cdot\ln x_{ZrO_2})+{^EG^{\varphi}}, \quad (3)$$

where the parameters $^{\circ}G^{\varphi}_{PbO}$, $^{\circ}G^{\varphi}_{TiO_2}$, $^{\circ}G^{\varphi}_{ZrO_2}$ represent the lattice stabilities of pure components and are given relative to the enthalpy of selected reference state of pure element at 298.15 K. The excess Gibbs free energy is expressed by the Redlich–Kister–Muggianu[88] polynomial

$$^EG^{\varphi}=x_{PbO}x_{TiO_2}\sum_{v=0}^{n}{^vL_{PbO,TiO_2}}(x_{PbO}-x_{TiO_2})^v+x_{PbO}x_{ZrO_2}\sum_{v=0}^{n}{^vL_{PbO,ZrO_2}}(x_{PbO}-x_{ZrO_2})^v+x_{TiO_2}x_{ZrO_2}\sum_{v=0}^{n}{^vL_{TiO_2,ZrO_2}}(x_{TiO_2}-x_{ZrO_2})^v+x_{PbO}x_{TiO_2}x_{ZrO_2}L_{PbO,TiO_2,ZrO_2}, \quad (4)$$

where $^vL_{i,j}$ (*i* and *j* are indexes which correspond to the species PbO, TiO_2 or ZrO_2) and L_{PbO,TiO_2,ZrO_2} are the binary and ternary interaction parameters, respectively. $v=0$, 1, 2...*n* is degree of interactions between the constituents or species, i.e., between first-, second-neighbours, etc. Increasing *v* indicates the increase of non-ideality of the system and usually it does not exceed 2. The ternary interaction term has the following composition dependence: $L_{PbO,TiO_2,ZrO_2}=x_{PbO}{^0L_{PbO,TiO_2,ZrO_2}}+x_{TiO_2}{^1L_{PbO,TiO_2,ZrO_2}}+x_{ZrO_2}{^2L_{PbO,TiO_2,ZrO_2}}$. In this work $^0L_{PbO,TiO_2,ZrO_2}$, $^1L_{PbO,TiO_2,ZrO_2}$ and $^2L_{PbO,TiO_2,ZrO_2}$ are equal, i.e. only a single parameter with a degree of zero is optimized.

Table 2. Selection of Experimental Information for the PbO–TiO_2–ZrO_2 System: Phase Diagram Data

Reference	Experimental Technique	Measured quantity, temperatures, compositions
18)	X-ray diffraction, Quenching	Liquidus and subsolidus of the quasibinary PbO-ZrO_2 section. Phase relations in the PbO-ZrO_2-TiO_2 system: isothermal, isobaric sections at 1373, 1473 and 1573 K in air; liquidus and solidus of $PbZrO_3$-$PbTiO_3$ section.
28)		Liquidus and subsolidus of the quasibinary PbO-TiO_2 system.
29)	X-ray diffraction, DTA (Differential thermal analysis) and themogravimetry, Thermobalance (by molar ratio O/Pb)	Air isobar of the PbO_x-TiO_2 and ternary TiO_2-PbO_2-Pb system. Subsolidus phase relations and stability range of phases based on the dissociation curves using the thermobalance to follow equilibrium loss in O/Pb weight. Stability range of intermediate phases ($PbTiO_3$ and $PbTi_3O_7$) below 973 K.
43)	X-ray diffraction, Neutron powder diffraction	Subsolidus of the quasybinary ZrO_2-TiO_2 section. Phase relations between 1273 and 1773 K. Stability range of $ZrTiO_4$ and $ZrTi_2O_6$ phases.
44)	X-ray diffraction, Rietveld analysis	Subsolidus of the quasibinary ZrO_2-TiO_2 section: Stability and homogeneity range of the ordered and disordered $ZrTiO_4$ phases; phase boundaries of titania and zirconia solid solutions and intermediate ($ZrTiO_4$) phases.
50)	X-ray diffraction, Optical pyrometry	Liqudus and solidus of the quasibinary ZrO_2-TiO_2 section.
53)	X-ray diffraction	Subsolidus phase relations in the ZrO_2-TiO_2 quasibinary at 1253 and 1643 K.
55)	X-ray diffraction, DTA, Optical microscopy, Chemical analysis	Subsolidus phase relations in the system PbO-ZrO_2-TiO_2 at 1373 K; Zirconia rich part of ZrO_2-TiO_2 quasibinary system: Solvus of monoclinic-tetragonal transformation and solubility of titania in zirconia solid solution in the temperature range 873-1373 K.
56)	Brightness pyrometry in the solar furnace (cooling curves)	Liquidus of the quasibinary ZrO_2-TiO_2 system.
57)	Brightness pyrometry in the heliostat-type solar furnace Quenching, X-ray diffraction	Liquidus of the quasibinary ZrO_2-TiO_2 system; Solid solution boundaries at lower temperature: phase boundary of the monoclinic and tetragonal zirconia solid solutions.
58)	High temp. X-ray diffraction, DTA	Zirconia rich part of ZrO_2-TiO_2 quasibinary system: Solvus of monoclinic-tetragonal transformation of zirconia solid solutions.
59)	X-ray diffraction, DTA	Liquidus and solidus of the quasibinary ZrO_2-TiO_2 system.
60)	X-ray diffraction,DTA	Subsolidus of the quasybinary ZrO_2-TiO_2 section. Metastable phase relationships. Homogenity range of $ZrTiO_4$ phase.
61)	X-ray diffraction, Rietveld analysis	Subsolidus of the quasibinary ZrO_2-TiO_2 section; Solvus of monoclinic-tetragonal transformation of the zirconia solid solutions; stability and homogeneity range of the ordered and disordered intermediate phases; phase boundaries of titania and zirconia solid solutions and intermediate ($ZrTiO_4$) phases.
64)	X-ray diffraction, Quenching	Liquidus and solidus of $PbZrO_3$-$PbTiO_3$ section.

The compound $\beta Zr_xTi_{1-x}O_4$ shows the homogeneity range in the quasibinary ZrO_2–TiO_2 section toward both the titania and zirconia solid solutions. In the present work, it is treated as a non-stoichiometric phase. According to the crystal structure,[46] there is only one crystallographic position for the metal atoms, which is shared by Ti and Zr. This phase is modelled using the substitutional solution model (TiO_2, ZrO_2). The same model is adopted for the description of titania and zirconia solid solutions. The Gibbs energy of $\beta Zr_xTi_{1-x}O_4$, titania and zirconia solid solutions is represented by Eqs. (3) and (4).

The cubic high temperature form of $PbZr_xTi_{1-x}O_3$, solid solution is described using the substitutional model ($PbTiO_3$, $PbZrO_3$). Similar to $\beta Zr_xTi_{1-x}O_4$, titania and zirconia solid solutions, in $PbZr_xTi_{1-x}O_3$ solid solutions one crystallographic position is shared by Ti and Zr.[66] The Gibbs energy of the end-members is expressed by Eq. (1) and for the solid solutions is given by following:

$$G = x_{PbTiO_3}\,{}^{\circ}G^{\beta\text{-}PbZr_xTi_{1-x}O_3}_{PbTiO_3} + x_{PbZrO_3}\,{}^{\circ}G^{\beta\text{-}PbZr_xTi_{1-x}O_3}_{PbZrO_3} + R\cdot T(x_{PbTiO_3}\ln x_{PbTiO_3} + x_{PbZrO_3}\ln x_{PbZrO_3}) + {}^{E}G^{\beta\text{-}PbZr_xTi_{1-x}O_3} \quad (5)$$

${}^{E}G^{\beta\text{-}PbZr_xTi_{1-x}O_3}$ is the excess term:

$${}^{E}G^{\beta\text{-}PbZr_xTi_{1-x}O_3} = x_{PbTiO_3}x_{PbZrO_3}\sum_{v=0}^{n}{}^{v}L_{PbTiO_3,\,PbZrO_3} \times (x_{PbTiO_3} - x_{PbZrO_3})^{v} \quad (6)$$

Phase equilibria in the PbO–TiO_2 system are accepted from

Table 3. Selection of Experimental Information for the $PbO-TiO_2-ZrO_2$ System: Thermodynamic Data

Reference	Experimental Tecnique	Measured quantity, temperatures, compositions
19)	EMF (electromotive force measurements)	Gibbs energy of formation of $PbZrO_3$ compound between 1073 – 1673 K.
21)	DSC (differential scanning calorimetry)	Specific heat of the $PbZrO_3$ compound in the temperature range 400 – 480 K.
23)	EMF Knudsen effusion	Gibbs energy of formation of $PbTiO_3$ and $PbZrO_3$ compounds in the temperature range 673 – 946 K. PbO potential above the lead titanate, lead zirconate and $Pb(Ti_{1-x}Zr_x)O_3$ solid solutions in the temperature range 673 – 1300 K.
24)	Knudsen effusion	PbO potential above the lead titanate, lead zirconate and $Pb(Ti_{1-x}Zr_x)O_3$ solid solutions in the temperature range 1073 – 1350 K.
25)	Knudsen effusion	PbO potential above the lead titanate, lead zirconate and $Pb(Ti_{1-x}Zr_x)O_3$ for x=0.5 in the temperature range 1073 – 1350 K; Nonstoichiometry of lead zirconate-lead titanate: Lead oxide, titania and zirconia activities as functions of composition in the lead-titanate and lead-zirconate single phase region; Activity coefficient of PbO as a function of $Pb(Ti_{1-x}Zr_x)O_3$ composition at 1373 and 1473 K.
26)	Knudsen effusion	Lead oxide activity above the lead titanate, lead zirconate and $Pb(Ti_{1-x}Zr_x)O_3$ solid solutions in the temperature range 1000 – 1350 K.
27)	Solution calorimetry Drop solution calorimetry	Enthalpy of formation of the lead titanate, lead zirconate and $Pb(Ti_{1-x}Zr_x)O_3$ solid solutions and heat of mixing at 973 K.
38)	EMF	Gibbs energy of formation of $PbTiO_3$ compound in the temperature range 1073 – 1273 K.
39)	EMF	Gibbs energy of formation of $PbTiO_3$ compound in the temperature range 1075 – 1350 K.
40)	High-temp. DSC	Specific heat of the $PbTiO_3$ compound in the temperature range 323 – 1273 K, enthalpy and entropy of tetragonal – cubic phase transition.
63)	Adiabatic calorimetry Solution calorimetry	Specific heat of the $ZrTiO_4$ compound in the temperature range 13 – 400 K; Enthalpy of formation at 973 and 1073 K.

the work of Rase et al.,[28] except the PbO-rich side. The Gibbs energy of the tetragonal and cubic lead titanate is based on the most recent experimental information. Similarly to the previous work[2] only high-temperature $PbZrO_3$ phase is included in the assessment of $PbO-ZrO_2$ system. The present assessment of ZrO_2-TiO_2 system is mainly based on the most recent and extensively investigated phase diagram published by Troitzsch et al..[61] The thermodynamic data for the $ZrTiO_4$ compound are used together with the determined phase boundaries of the two phase regions zirconium titanate + zirconia solid solutions and zirconium titanate + titania solid solutions. Both, low- and high-temperature $ZrTiO_4$ phases are included in the assessment and in view of insufficient experimental information, they are modelled as separate phases. In addition, the solubility of titania in the monoclinic zirconia is based on the carefully selected experimental data, while the homogeneity range of the cubic zirconia is estimated.

4. Results and discussion

The optimization is done using the module PARROT included in the software package for thermodynamic calculations "Thermo-Calc."[9] The resulting set of parameters is shown in **Table 4**. By expanding the interaction parameters to higher order terms a better fit might be obtained with experimental data. However, the experimental data themselves are not conclusive enough and, therefore, the introduction of higher order terms (particularly for the liquid phase, ${}^1L$ and ${}^2L$) was not considered.

The calculated phase diagrams of the binary $PbO-TiO_2$, $PbO-ZrO_2$ and ZrO_2-TiO_2 systems are presented on the **Figs. 1**, **2** and **3** (a, b and c), respectively.

The Gibbs energy of both, tetragonal $\alpha PbTiO_3$ and cubic $\beta PbTiO_3$ modifications are evaluated in the present work (**Table 5**). The thermodynamic properties of lead titanate differ significantly from those reported in the modelling work of Soh et al.[3] based on the estimated values of heat capacity. **Figure 4** shows the comparison of the calculated and experimentally measured heat capacity of lead titanate reported by Rossetti et al..[40] Due to insufficient number of experimental data points at temperatures below the phase transformation $\alpha PbTiO_3 \rightarrow \beta PbTiO_3$, the heat capacities of both phases are taken to be equal. Calculated and experimentally measured thermodynamic properties of lead zirconate are also shown in Table 5. Since the heat content of $\beta PbZrO_3$ is not known, it is described using the Neumann–Kopp rule, while good agreement between calculated and measured enthalpy of formation[27] is obtained. Enthalpy of formation and entropy of $\beta Zr_xTi_{1-x}O_4$ at 298 K are in good agreement with data reported by Hom et al..[63] Heat capacity was measured up to 400 K, while the data above this temperature up to 1800 K were extrapolated.[63] Since extrapolated data are not considered in this work and there are only few measured points above 298 K, the heat capacity of $\beta Zr_xTi_{1-x}O_4$ is described by the Neumann–Kopp rule that shows good fit with the measured data up to 400 K (**Fig. 5**). Calculated partial pressure of lead oxide over $\beta PbTiO_3$ is in good agreement with data reported by Schmahl et al.,[23] Haerdtl and Rau[24] and Holman and Fulrath[25] (**Fig. 6**), while the data of Popovic et

Table 4. Summary of the Thermodynamic Parameters Describing the PbO–TiO_2–ZrO_2 System Referred to Stable Element Reference H^{SER}

∗ : This work

Parameter	Equation	Reference
Liquid (PbO, TiO_2, ZrO_2)		
${}^{o}G^{liq}_{PbO}$	(3)	84)
${}^{o}G^{liq}_{ZrO_2}$	(3)	85)
${}^{o}G^{liq}_{TiO_2}$	(3)	86)
${}^{0}L^{liq}_{PbO,ZrO_2} = -4600$	(4)	∗
${}^{0}L^{liq}_{PbO,TiO_2} = 124200 + 52.2\,T$	(4)	∗
${}^{1}L^{liq}_{PbO,TiO_2} = 16900$	(4)	∗
${}^{0}L^{liq}_{ZrO_2,TiO_2} = -170653.79 + 67.49\,T$	(4)	∗
${}^{1}L^{liq}_{ZrO_2,TiO_2} = +23686.45$	(4)	∗
${}^{2}L^{liq}_{ZrO_2,TiO_2} = -25941.76$	(4)	∗
${}^{0}L^{liq}_{PbO,ZrO_2,TiO_2} = 60582.55$	(4)	∗
αPbO (PbO,TiO_2,ZrO_2)		
${}^{o}G^{\alpha PbO}_{PbO}$	(3)	84)
${}^{o}G^{\alpha PbO}_{TiO_2} = GTiO_2 + 40000$	(3)	∗
${}^{o}G^{\alpha PbO}_{ZrO_2} = GZrO_2M + 40000$	(3)	∗
${}^{0}L^{\alpha PbO}_{PbO,ZrO_2} = -30000$	(4)	∗
${}^{0}L^{\alpha PbO}_{PbO,TiO_2} = -60000$	(4)	∗
βPbO		
${}^{o}G^{\beta-PbO}_{PbO}$	(1)	84)
Rutile -TiO_2 (TiO_2, ZrO_2)		
${}^{o}G^{rutile}_{TiO_2}$	(3)	86)
${}^{o}G^{rutile}_{ZrO_2} = GZrO_2T + 35000$	(3)	∗
${}^{0}L^{rutile}_{TiO_2,ZrO_2} = 3400 - 11.95\,T$	(4)	∗
${}^{1}L^{rutile}_{TiO_2,ZrO_2} = 3402 + 6.2\,T$	(4)	∗
αZrO_2 (ZrO_2, TiO_2)		
${}^{o}G^{\alpha-ZrO_2}_{ZrO_2}$	(3)	85)
${}^{o}G^{\alpha-ZrO_2}_{TiO_2} = GTiO_2 + 7330$	(3)	∗
${}^{0}L^{\alpha-ZrO_2}_{ZrO_2,TiO_2} = 30245 - 4.1\,T$	(4)	∗
βZrO_2 (ZrO_2, TiO_2)		
${}^{o}G^{\beta-ZrO_2}_{ZrO_2}$	(3)	85)
${}^{o}G^{\beta-ZrO_2}_{TiO_2} = GTiO_2 + 35000$	(3)	∗
${}^{0}L^{\beta-ZrO_2}_{ZrO_2,TiO_2} = -16868.73 - 6.26\,T$	(4)	∗
${}^{1}L^{\beta-ZrO_2}_{ZrO_2,TiO_2} = -4439.5 - 11.75\,T$	(4)	∗
γZrO_2 (ZrO_2, TiO_2)		
${}^{o}G^{\gamma-ZrO_2}_{ZrO_2}$	(3)	85)
${}^{o}G^{\gamma-ZrO_2}_{TiO_2} = GTiO_2 + 35000$	(3)	∗
${}^{0}L^{\gamma-ZrO_2}_{ZrO_2,TiO_2} = 5740 - 6.26\,T$	(4)	∗
β$ZrTiO_4$ (TiO_2, ZrO_2)		
${}^{o}G^{\beta-TiZrO_4}_{TiO_2} = GTiO_2 + 6000$	(3)	∗
${}^{o}G^{\beta-TiZrO_4}_{ZrO_2} = GZrO_2T + 6000$	(3)	∗
${}^{0}L^{\beta-TiZrO_4}_{TiO_2,ZrO_2} = 7707.8 - 1.95\,T$	(4)	∗
β$PbZr_xTi_{1-x}O_3$ ($PbTiO_3$, $PbZrO_3$)		
${}^{o}G^{\beta-PbZr_xTi_{1-x}O_3}_{PbTiO_3} = GPbTiO_3C$	(5)	∗
${}^{o}G^{\beta-PbZr_xTi_{1-x}O_3}_{PbZrO_3} = GZrO_2M + GPBOYEL - 10.71\,T$	(5)	∗
${}^{o}L^{\beta-PbZr_xTi_{1-x}O_3}_{PbTiO_3,PbZrO_3} = 8.037\,T$	(6)	∗
α′$PbTiO_3$		
${}^{o}G^{\alpha'-PbTiO_3}_{PbTiO_3} = GPbTiO_3T$	(1)	∗
α$ZrTiO_4$		
${}^{o}G^{\alpha-ZrTiO_4}_{ZrO_2:TiO_2} = GTiO_2 + GZrO_2T + 3200 - 3.63\,T$	(1)	∗
$ZrTi_2O_6$		
${}^{o}G^{TiZr_2O_6}_{ZrO_2:TiO_2} = 2\,GTiO_2 + GZrO_2M - 12100 + 7.9\,T$	(1)	∗
$GPbTiO_3T = -1241000 + 745.856\,T - 127.086\,T\ln T + 609829.18\,T^{-1}$	(1)	∗
$GPbTiO_3C = -1239466.5 + 743.544\,T - 127.086\,T\ln T + 609829.18\,T^{-1}$	(1)	∗

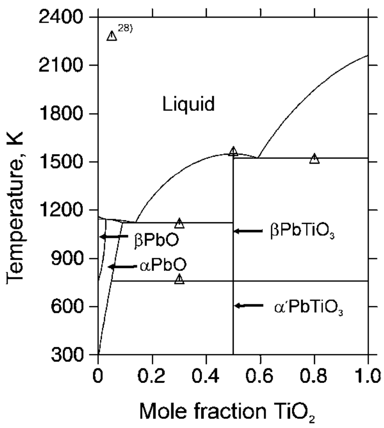

Fig. 1. Calculated PbO–TiO_2 phase diagram in comparison with the experimental data.[28]

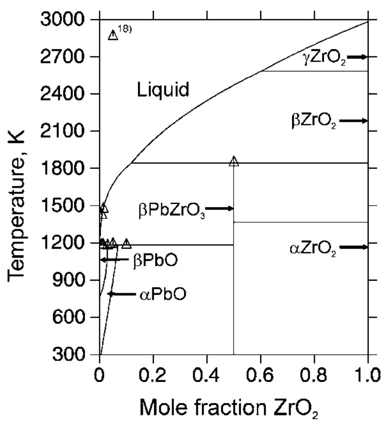

Fig. 2. Calculated PbO–ZrO_2 phase diagram compared with experimental measurements.[18]

al.[26] are inconsistent with the selected experimental information in $PbO–TiO_2$ system. The calculated partial pressure of lead oxide over $\beta PbZrO_3$ fits well the data reported by Popovic et al.[26] and Jacob and Shim,[19] while the results of other authors[23)–25)] are inconsistent with the phase diagram reported by Fushimi and Ikeda.[18] The agreement between calculated and measured values for the $\beta PbZr_xTi_{1-x}O_3$ solid solutions[23)–26)] is quite satisfactory. The data obtained by Knudsen technique[23)–26)] have been partially used in optimization (the partial pressure reported by Popovic et al.[26] was measured over the nonequilibrated phases for the most of investigated compositions).

The calculated invariant equilibria in the $PbO–TiO_2$ system compared with the experimental ones are presented in **Table 6**. The peritectic reaction Liquid + βPbO→αPbO occurs at 1145 K and 2.75 mol.% TiO_2 dissolved in tetragonal αPbO solid solution (Table 6). Matsuo and Sasaki[89] reported that orthorhombic βPbO dissolves some TiO_2 and converted itself to tetragonal αPbO. This finding is in accordance with the tentatively drawn solubility of TiO_2 (less than 2 mol.%) in βPbO by Rase et al..[28] Since, the solubility of TiO_2 in βPbO phase is probably very small, it is not taken in account in the present work. In addition, the thermodynamic and phase boundary data for αPbO and βPbO are missing.

$\beta PbZrO_3$ compound melts incongruently at 1842.54 K and 88.14 mol.% PbO (**Table 7**). The calculated maximal solubility of zirconia in tetragonal, αPbO, solid solution is 6.98 mol.% at temperature 1180 K of peritectic reaction Liquid + $\beta PbZrO_3$→αPbO, while the experimentally measured one at 1125 K is about 4 mol.% ZrO_2.[90] PbO-rich side of $PbO–ZrO_2$ phase diagram (Fig. 2) differs from the one reported by Fushimi and Ikeda,[18] but it is similar to the assessed phase relations by Koo et al..[2] Predicted eutectic reaction, Liquid→ αPbO + βPbO take place at 0.033 mol.% ZrO_2 and temperature at 1158.70 K, what is just below the melting point of βPbO at 1158.84 K.

The calculated invariant equilibria in the $ZrO_2–TiO_2$ system are compared with the experimental ones in **Table 8.** Agree-

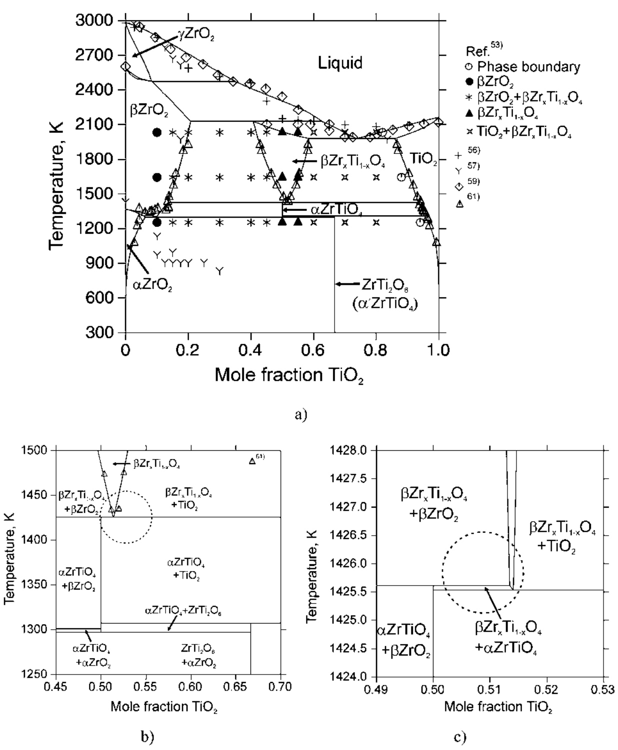

Fig. 3. Calculated $ZrO_2–TiO_2$ phase diagram with the corresponding experimental points (a) and enlarged view of the central part of diagram (b, c).

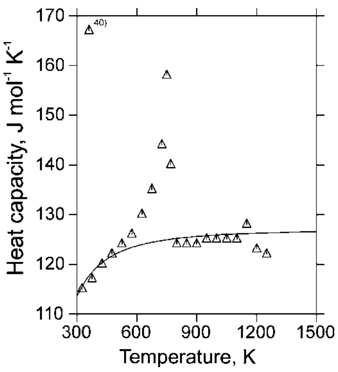

Fig. 4. Comparison of the calculated and measured heat capacity of lead titanate.

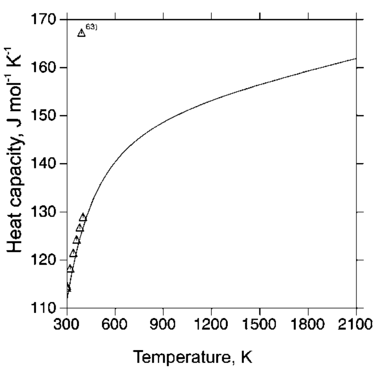

Fig. 5. Comparison of the calculated and measured heat capacity of $\beta Zr_xTi_{1-x}O_4$.

Table 5. Calculated and Experimentally Measured Thermodynamics Functions (Δ_fH°, ΔS° and Δ_fG° are the enthalpy, entropy and Gibbs energy of formation, respectively) of α' $PbTiO_3$, β $PbZrO_3$ and β $Zr_xTi_{1-x}O_4$ compounds at 298.15 K

Compound	Δ_fH° [kJ·mol^{-1}]	ΔS° [J·mol^{-1}·K^{-1}]	Δ_fG° [kJ·mol^{-1}]	Reference
$\alpha' PbTiO_3$	-1199.02	112.47	-1232.55	This work
	-1199.74 ± 2.88			27)
$\beta PbZrO_3$	-1318.00	129.19	-1356.51	This work
	-1319.18 ± 4.66			27)
$\beta Zr_xTi_{1-x}O_4$ (x = 0.5)	-2024.01	116.22	-2058.66	This work
	-2024.1± 4.5	116.71 ± 0.31		63)

ment between calculated and experimental data is very good, except in the ZrO_2-rich side near to eutectoid reaction $\beta ZrO_2 \rightarrow \alpha ZrO_2 + \alpha ZrTiO_4$ which occurs at somewhat lower temperature than suggested in. Refs.[58),61)] On the other hand, Webster et al.[55)] as well as Noguchi and Mizuno[57)] found significantly lower reaction temperature (923 K), what is probably due to the shorter annealing time in their experiments. Consequently, at low temperatures the kinetic is very sluggish and equilibri-

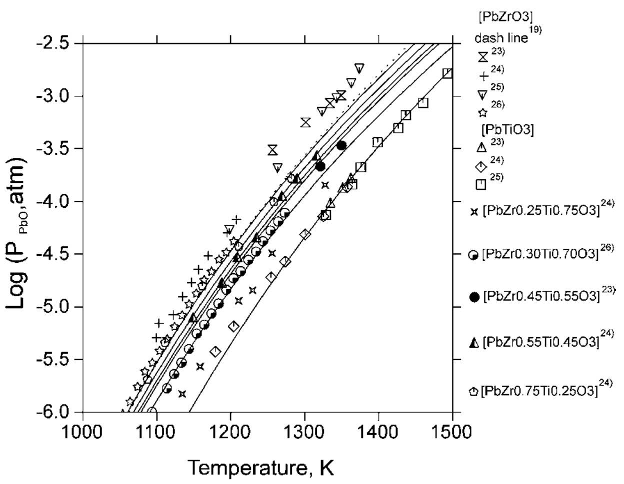

Fig. 6. Calculated and measured partial pressure of lead-oxide over the end members, $\beta PbZrO_3$, $\beta PbTiO_3$ and $\beta PbZr_xTi_{1-x}O_3$ solid solutions superimposed with experimental measurements.

Table 6. Invariant Equilibria in the PbO–TiO_2 System

Reaction, mol. % TiO_2					Type	T (K)	Reference
L	↔	$\beta PbTiO_3$	+	TiO_2	Eutectic		
59.03					e_2	1522.97	This work
59.00±0.1						1513	28)
L	↔	$\beta PbTiO_3$			Congruent		
						1551.61	This work
						1558	28)
L	↔	$\beta PbTiO_3$	+	αPbO	Eutectic		
13.77				8.95	e_3	1124.19	This work
13.80±0.1				-		1111	28)
L	+	βPbO	↔	αPbO	Peritectic		
3.10				2.75	p_3	1145.06	This work
$\alpha PbTiO_3$	↔	$\beta PbTiO_3$			Solid-state transform.	760.81	This work
						760±2	40)

Table 7. Invariant Equilibria in the PbO–ZrO_2 System

Reaction, mol. % ZrO_2					Type	T (K)	Reference
L	+	γZrO_2	↔	βZrO_2	Peritectic		
60.18					p_4	2584.00	This work
L	+	βZrO_2	↔	$\beta PbZrO_3$	Peritectic		
11.86					p_5	1842.54	This work
-						1843	18)
L	+	$\beta PbZrO_3$	↔	αPbO	Peritectic		
0.12				6.98	p_6	1181.80	This work
< 1.00				-		1183	18)
-				4.00		-	90)
L	↔	αPbO	+	βPbO	Eutectic		
0.033		2.95			e_4	1158.70	This work

Table 8. Invariant Equilibria in the ZrO_2–TiO_2 System

Reaction, mol. % TiO_2					Type	T (K)	Reference
L	↔	$\beta Zr_xTi_{1-x}O_4$	+	TiO_2	Eutectic		
73.70		58.60		85.98	e_1	1978.32	This work
80.00		~ 60		~ 85		2033	50)
75.30		-		-		1973	57)
73.00		-		~ 82		1993±20	59)
L	+	βZrO_2	↔	$\beta Zr_xTi_{1-x}O_4$	Peritectic		
62.62		20.75		40.71	p_1	2128.70	This work
55.00		-		50.00		2093	50)
52.00		-		-		2093	57)
60.00		-		-		2143	59)
L	+	γZrO_2	↔	βZrO_2	Peritectic		
34.99		8.32		8.45	p_2	2473.41	This work
16.70		-		-		2616	57)
35.00		-		-		2473	59)
βZrO_2	↔	αZrO_2	+	$\alpha ZrTiO_4$	Eutectoid		
9.89		6.30		50.00		1300.94	This work
-		12		($ZrTi_2O_6$?)		923	57)
-		5		(TiO_2)		1354	58)
~ 12		~ 9		~ 49		1357	61)
$ZrTi_2O_6$	↔	$\alpha ZrTiO_4$	+	TiO_2	Peritectoid		
66.67		50.00		95.42		1307.2	This work
~ 67		(β $ZrTiO_4$)		-		~ 1473	43)
~ 61		50.00		94.84		~ 1340	61)
$\beta Zr_xTi_{1-x}O_4$	↔	$\alpha ZrTiO_4$	+	TiO_2	Eutectoid		
51.41		50.00		93.41		1425.41	This work
51.35		49.45		93.48		~ 1420	61)

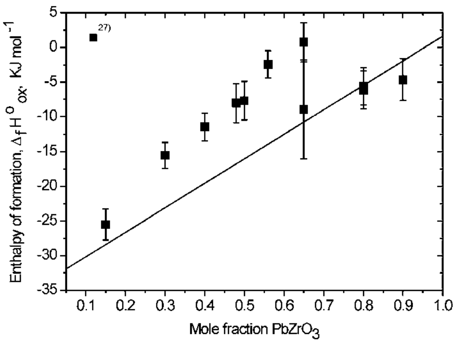

Fig. 7. Calculated enthalpy of formation of the $\beta PbZr_xTi_{1-x}O_3$ solid solutions from oxides at 298 K in comparison with experimental measurements.[27)]

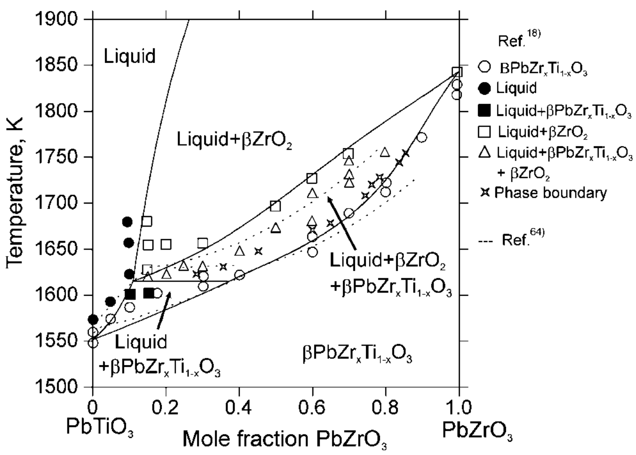

Fig. 8. Calculated $PbTiO_3$–$PbZrO_3$ section as compared with experimental measurements.

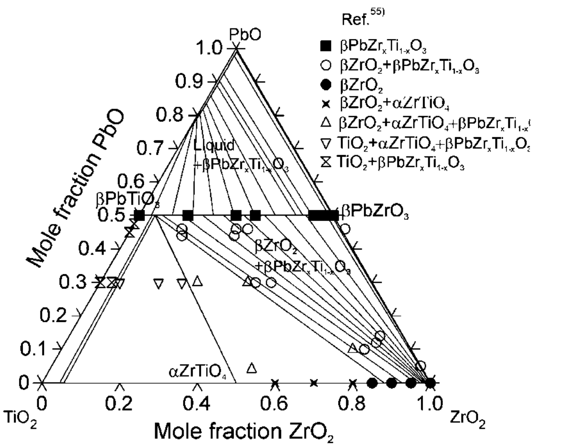

Fig. 9. Isothermal section of the PbO–ZrO_2–TiO_2 phase diagram at 1373 K compared with experimental measurements.

um is not reached. Measured solubility of titania in βZrO_2 up to 1900 K[61),91)] supports the calculated value of 20.75 mol.% at the temperature of 2128.70 K for the peritectic reaction Liquid + $\beta ZrO_2 \rightarrow \beta Zr_xTi_{1-x}O_4$ obtained in the present work (Table 8). The calculated solubility of titania in αZrO_2 is 6.3 mol.% at the eutectoid temperature, what is close to the results reported by Ono[58)] (Table 8). The ZrO_2-rich part of the phase diagram above 2500 K, except the liquidus, is estimated in the present work. Due to the difficulties in conducting experiments at such high temperatures no reliable information in this region could be taken into account. Experimentally registered anomalies on the liquidus curve[56),59)] are well consistent with calculations. These anomalies correspond to the peritectic reactions, p_2 and p_1 shown in Table 8. The calculated liquidus is consistent with the data of Shevchenko et al.,[59)] while the other measurement of the liquidus in the ZrO_2–TiO_2 system[56)] shows large negative deviations.

Figure 7 shows the calculated enthalpy of formation of the $\beta PbZr_xTi_{1-x}O_3$ solid solutions from oxides at 298 K as compared with experimental data of Rane and Navrotsky.[27)] The measured enthalpies show the regular mixing behavior with the uncertainty of measurements, which is sometime higher than the measured values. However, when extrapolating these data to high temperatures the phase relations become inconsistent with the selected experimental information in the present work and the behavior of the ideal mixing is accepted. Nevertheless, the agreement between calculation and experiment is quite good. The calculated section $PbTiO_3$–$PbZrO_3$ is shown in **Fig. 8**. The $PbTiO_3$–$PbZrO_3$ system cannot be rigorously treated as a quasibinary one and this phase diagram is an interesting example, in which a congruently melting and an incongruently melting compound form a solid solution over the entire range of composition. The diagram includes experimental results from different reports.[18),64)] Deviation between calculations and experimental data is within the uncertainty of measurements. The calculated isothermal section at 1373 K (**Fig. 9**) is consistent with those reported in literature.[55),90)] The nonstoichiometry of the lead titanate–lead zirconate solid solution,[25),90)] i.e., the deviation from the ratio $PbO/(ZrO_2 + TiO_2) = 1$ is not taken in account in the present work. In the region, where the PbO content is more than 50 mol.%, the calculated isothermal sections at 1373, 1473 and 1573 K and the tie lines (**Figs. 10a**, b and c) are compared with the experimentally determined ones.[18)] Isothermal lines are close and almost parallel to the PbO–TiO_2 side. At lower temperatures, the solubility of the ZrO_2 in the liquid phase increases with increasing $PbZrO_3$ content (Figs. 10a and b), while it is almost constant at 1573 K (Fig. 10c). Such trend is consistent with the results of Fushimi and Ikeda.[18)] The calculated projection of the monovariant liquidus lines is shown in **Figs. 11a** and b. According to the present work, the solidification sequence in the PbO–TiO_2–ZrO_2 system is in agreement with the schematically proposed polythermal projection by Fushimi and Ikeda,[18)] where the solubility surface for zirconia dominates in the system. The calculated invariant reactions (**Table 9**) are consistent with those estimated in literature.[18)]

5. Summary

Thermodynamic properties of the ternary PbO–ZrO_2–TiO_2 system are analyzed by means of the CALPHAD method. The parameters describing the boundary systems PbO–TiO_2, PbO–ZrO_2 and ZrO_2–TiO_2 are evaluated in the present work. The liquid phase is modeled by the solution model using ternary interaction parameters. The ternary compounds, $PbZrO_3$ and $PbTiO_3$ are modeled as a stoichiometric phase, while the solution model is adopted for the description of non-stoichiometry of the $\beta Zr_xTi_{1-x}O_4$, $\beta PbZr_xTi_{1-x}O_3$, titania and zirconia solid solutions.

The relevant literature information is critically assessed and the inconsistencies are revealed. A self-consistent set of Gibbs energy functions describing the phases in the PbO–ZrO_2–TiO_2

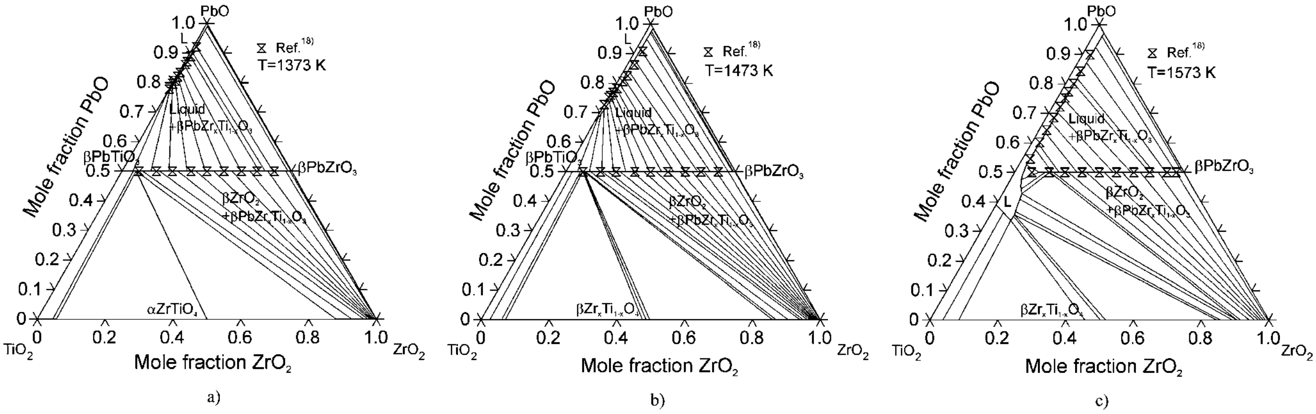

Fig. 10. Isothermal sections of the $PbO-ZrO_2-TiO_2$ phase diagram and the tie lines at 1373 (a), 1473 (b) and 1573 (c) in comparison with the experimental data.

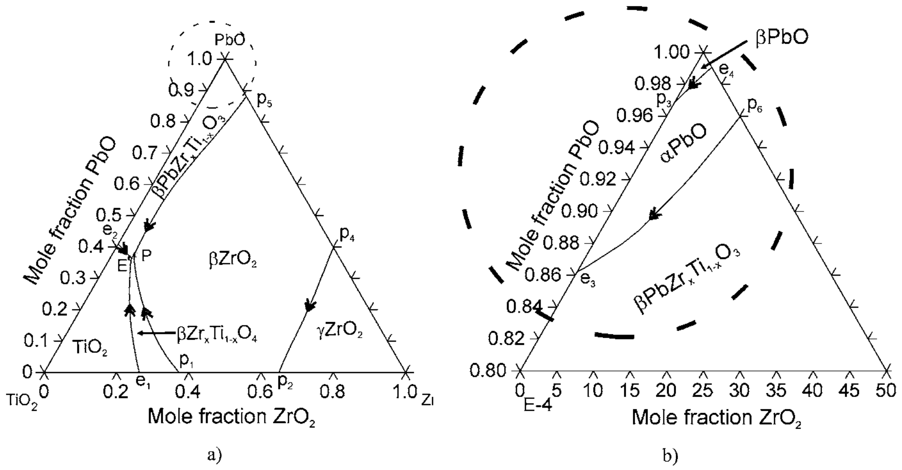

Fig. 11. Calculated projection of the monovariant liquidus lines in the ternary $PbO-ZrO_2-TiO_2$ system (a) and magnified PbO-rich part (b). Fields of primary crystallization are indicated.

Table 9. Invariant Equilibria in the Ternary $PbO-TiO_2-ZrO_2$ System (Temperatures in Parentheses* are Estimated by Fushimi and Ikeda[18])

		Reaction, mol. % ZrO_2 mol. % PbO					Type	*T* (K)
L	+	βZrO_2	↔	$\beta Zr_xTi_{1-x}O_4$	+	$\beta PbZr_xTi_{1-x}O_3$	Peritectic	
6.11		85.13		51.00		6.36	P	1531.66
37.41		0		0		50.00		*(1573)
L	↔	TiO_2	+	$\beta Zr_xTi_{1-x}O_4$	+	$\beta PbZr_xTi_{1-x}O_3$	Eutectic	
5.81		7.82		46.61		5.32	E	1521.62
36.60		0		0		50.00		*(1503)

system is obtained by least-squares fits to the selected experimental data. The backward compatibility of the refined parameters with the preferred datasets is demonstrated by calculation of various phase diagrams and thermodynamic properties, such as isothermal sections, vertical sections, and partial pressure, which are compared with literature data.

References

1) Čančarević, M., Zinkevich, M. and Aldinger, F., "Evaluation of the O–Pb–Zr System," Ed. by Effenberg, G., Phase Equilibria of Ternary Alloys, Landolt–Börnstein, Springer, submitted.
2) Koo, B. K., Liang, P., Seifert, H. J. and Aldinger, F., *Korean J. Ceram.*, Vol. 5, No. 3, pp. 205–210 (1999).
3) Soh, J. R., Lee, H. M. and Kwon, H. S., *Calphad*, Vol. 18, No. 3, pp. 237–244 (1994).
4) Yokokawa, H., Sakai, N., Kawada, T. and Dokiya, M., Int. Conf. Sci. Technol. Zirconia V, Melbourne, Australia, August 16–21, pp. 59–68 (1992), Ed. by Badwal, S. P. S., Bannister, M. and Hannink, R. H. J., Technomic Publishing, Lancaster, Pennsylvania (1993) pp. 59–68.
5) Gong, W., Jin, Z. and Du, Y., *J. Min. Met.*, Vol. 36B, No. 3–4, pp. 123–132 (2000).

6) Park, J. H., Liang, P., Seifert, H. J., Aldinger, F., Koo, B. K. and Kim, H. G., *Korean J. Ceram.*, Vol. 7, No. 1, pp. 11–15 (2001).
7) Kaufman, L., *Calphad*, Vol. 25, pp. 141–161 (2001).
8) Spencer, P. J., *Calphad*, Vol. 25, pp. 163–174 (2001).
9) Andersson, J. O., Helander, T., Hoglund, L., Shi, P. and Sundman, B., *Calphad*, Vol. 26, pp. 273–312 (2002).
10) Teslic, S. and Egami, T., *Acta Crystallogr., Sect. B: Struct. Crystallogr. Crys. Chem.*, Vol. B54, pp. 750–765 (1998).
11) Tanaka, M., Saito, R. and Tsuzuki, K., *J. Phys. Soc. Jpn.*, Vol. 51, pp. 2635–2640 (1982).
12) Sawaguchi, E., Maniwa, H. and Hoshino, S., *Phys. Rev.*, Vol. 83, pp. 1078–1078 (1951).
13) Ujma, Z., Handerek, J. and Pisarski, M., *Ferroelectrics*, Vol. 64, pp. 237–245 (1985).
14) Boher, P., Garnier, P., Gavarri, J. R. and Hewat, A. W., *J. Solid State Chem.*, Vol. 57, pp. 343–350 (1985).
15) Hill, R. J., *Acta Crystall. C*, Vol. 41, pp. 1281–1284 (1985).
16) Winterer, M., Delaplane, R. and McGreevy, R., *J. Appl. Crystall.*, Vol. 35, pp. 434–442 (2002).
17) Bouvier, P., Djurado, E., Lucazeau, G. and Le Bihan, T., *Physical Review, Serie 3. B-Condensed Matter*, Vol. 62, pp. 8731–8737 (2000).
18) Fushimi, S. and Ikeda, T., *J. Am. Ceram. Soc.*, Vol. 50, No. 3, pp. 129–132 (1967).
19) Jacob, K. T. and Shim, W. W., *J. Am. Ceram. Soc.*, Vol. 64, pp. 573–578 (1981).
20) Harris, N. H., Ph. D. Thesis, University of Illinois, 1967; cited in Jacob, K. T. and Shim, W. W., *J. Am. Ceram. Soc.*, Vol. 64, pp. 573–578 (1981).
21) Gospodinov, G. G. and Marchev, V. M., *Thermochim. Acta*, Vol. 222, pp. 137–141 (1993).
22) Onodera, A., Kawamura, Y., Tamaki, N., Fujishita, H., Roleder, K., Dec, J. and Molak, A., *J. Korean Phys. Soc.* (Proc. Suppl.), Vol. 29, pp. S691–S694 (1996).
23) Schmahl, N. G., Schwitzgebel, G., Kling, H. and Speck, E., *Mat. Res. Bull.*, Vol. 14, pp. 1213–1218 (1979).
24) Haerdtl, K.H. and Rau, H., *Solid State Communication*, Vol. 7, pp. 41–45 (1969).
25) Holman, R. and Fulrath, R. M., *J. Appl. Phys.*, Vol. 44, No. 12, pp. 5227–5236 (1973).
26) Popovic, A., Malic, B. and Benceze, L., *Rapid Commun. Mass Spectrom.*, Vol. 13, pp. 1129–1137 (1999).
27) Rane, M.V. and Navrotsky, A., *J. Solid State Chem.*, Vol. 161, pp. 402–409 (2001).
28) Rase, D. E., cited in Jaffe, B., Cook, W. R. and Jaffe, H., "Piezoelectric Ceramics," Academic Press, London-New-York (1971) pp. 117–117.
29) Eisa, M. A., Abadir, M. F. and Gaddala, A. M., *Tran. J. Brit. Ceram. Soc.*, Vol. 79, pp. 100–104 (1980).
30) Robinson, A. E. and Joyce, T. A., *Trans. J. Brit. Ceram. Soc.*, Vol. 61, No. 2, pp. 85–85 (1962).
31) Belyaev, I. N., *Russ. J. Inorg. Chem.*, Vol. 15, No.1, pp. 148–149 (1970).
32) Sani, A., Hanfland, M. and Levy, D., *J. Solid State Chem.*, Vol. 167, pp. 446–452 (2002).
33) Ayakan, J., *J. Am. Ceram. Soc.*, Vol. 51, No. 10, pp. 577–582 (1968).
34) Gonschorek, W., *Z. f. Kristall.*, Vol. 160, pp. 187–203 (1982).
35) Burdett, J. K., Hughbanks, T., Miller, G. J., Richardson, J. W., Jr. and Smith, J. V., *J. Am. Chem. Soc.*, Vol. 109, pp. 3639–3646 (1987).
36) Meagher, E. P. and Lager, G. A., *Can. Mineralogist*, Vol. 17, pp. 77–85 (1979).
37) Kato, K., Kawada, I. and Muramatsu, K., *Acta Crystall. B*, Vol. 30, pp. 1634–1635 (1974).
38) Mehrotra, M. G., Frohberg, M. G., Mathew, P. M. and Kapoor, M. L., *Scripta Metall.*, Vol. 7, pp. 1047–1052 (1973).
39) Shim, W. W. and Jacob, K. T., *Can. Metall. Quarterly.*, Vol. 21, No. 2, pp. 171–177 (1982).
40) Rossetti, G. A. and Maffei, N., *J. Phys.: Condens. Matter.*, Vol. 17, pp. 3953–3963 (2005).
41) Barin, I., "Thermochemical Data of Pure Substances," VCH, Weinheim (1993) pp. 1157–1157.
42) McHale, A. E. and Roth, R. S., *J. Am. Ceram. Soc.*, Vol. 66, No. 2, pp. C18–C20 (1983).
43) McHale, A. E. and Roth, R. S., *J. Am. Ceram. Soc.*, Vol. 69, No. 11, pp. 827–832 (1986).
44) Troitzsch, U., Christy, A. G. and Ellis, D. J., *J. Am. Ceram. Soc.*, Vol. 87, No. 11, pp. 2058–2063 (2004).
45) Troitzsch, U., Ellis, D. J. and Christy, A. G., *Eur. J. Mineral.*, Vol. 16, pp. 577–584 (2004).
46) Bordet, P., McHale, A., Santoro, A. and Roth, R. S., *J. Solid. State Chem.*, Vol. 64, pp. 30–46 (1986).
47) Christofferson, R. and Davies, P. K., *J. Am. Ceram. Soc.*, Vol. 75, No. 3, pp. 563–569 (1992).
48) Dondi, M., Matteucci, F. and Cruciani, G., *J. Solid State Chem.*, Vol. 179, pp. 233–246 (2006).
49) Park, Y. and Kim, Y., *Mat. Res. Bullet.*, Vol. 31, No. 1, pp. 7–15 (1996).
50) Coughanour, L. W., Roth, R. S. and DeProsse, V. A., *J. Res. Natl. Bur. Stand.*, Vol. 52, No. 1, pp. 37–42 (1954).
51) Newnham, R. E., *J. Am. Ceram. Soc.*, Vol. 50, pp. 216–216 (1967).
52) Sowan, H. G. and Andrews, A. I., *J. Am. Ceram. Soc.*, Vol. 34, No. 10, pp. 298–301 (1951).
53) Brown, F. H. and Duwez, P., *J. Am. Ceram. Soc.*, Vol. 37, No. 3, pp. 129–132 (1954).
54) Cocco, A. and Torriano, G., *Ann. Chim.*, Vol. 55, No. 3, pp. 153–163 (1965).
55) Webster, A. H., McDonald, R. C. and Browman, W. S., *J. Can. Ceram. Soc.*, Vol. 34, pp. 97–102 (1965).
56) Noguchi, T. and Mizuno, M., *Sol. Energy*, Vol. 11, No. 1, pp. 56–61 (1967).
57) Noguchi, T. and Mizuno, M., *Bull. Chem. Soc. Jpn.*, Vol. 41, No. 12, pp. 2895–2899 (1968).
58) Ono, A., *Mineral J.*, Vol. 6, No. 6, pp. 433–441 (1972).
59) Shevchenko, A. V., Lopato, L. M., Maister, I. M. and Gorbunov, O. S., *Zh. Neorg. Khim.*, Vol. 25, No. 9, pp. 2496–2499 (1980); *Russ. J. Inorg. Chem.*, Vol. 25, No. 9, pp. 1379–1381 (1980).
60) Kobayashi, K., Kato, K., Terabe, K., Yamaguchi, S. and Iguchi, Y., *J. Ceram. Soc. Japan*, Vol. 106, No. 8, pp. 782–786 (1998).
61) Troitzsch, U. and Ellis, D. J., *J. Mat. Sci.*, Vol. 40, No. 17, pp. 4571–4577 (2005).
62) Buessem, W., Schusterius, C. and Ungewiss, A., *Ber. Dtsch. Keram. Ges.*, Vol. 18, No. 10, pp. 433–443 (1937).
63) Hom, B. K., Stevens, R., Woodfield, B. F., Baerio-Goates, J., Putnam, R. L., Helean, K. B. and Navrotsky, A., *J. Chem. Thermodynamics*, Vol. 33, pp. 165–178 (2001).
64) Moon, R. L. and Fulrath, R. M., *J. Am. Ceram. Soc.*, Vol. 54, No. 2, pp. 124–125 (1971).
65) Jaffe, B., Cook, W. R. and Jaffe, H., "Piezoelectric Ceramics," Academic Press, London-New-York (1971) pp. 135–135.
66) Glazer, A. M. and Mabud, S. A., *Acta Crystall. B*, Vol. 34, pp. 1060–1065 (1978).
67) Frantti, J., Lappalainen, J., Eriksson, S., Lantto, V., Nishio, S., Kakihana, M., Ivanov, S. and Rundlof, H., *Jpn. J.Appl. Phys.*, Part 1, Vol. 39, pp. 5697–5703 (2000).
68) Jirak, Z. and Kala, T., *Ferroelectrics*, Vol. 82, pp. 79–84 (1988).
69) Noheda, B., Gonzalo, J. A., Cross, L. E., Guo, R., Park, S. E., Cox, D. E. and Shirane, G., *Phys. Rev. B-Condens. Matter*, Vol. 61, No. 13, pp. 8687–8695 (2000).
70) Souza Filho, A. G., Lima, K. C. V., Ayala, A. P., Guedes, I., Freire, P. T. C., Mendes Filho, J., Araujo, E. B. and Eiras, J. A., *Phys. Rev. B*, Vol. 61, pp. 14283–14286 (2000).
71) Souza Filho, A. G., Lima, K. C. V., Ayala, A. P., Guedes, I., Freire, P. T. C., Mendes Filho, J., Araujo, E. B. and Eiras, J. A., *Phys. Rev. B*, Vol. 63, pp. 176103/1–176103/2 (2001).
72) Frantti, J., Lappalainen, J., Eriksson, S., Ivanov, S., Lantto,

V., Nishio, S., Kakihana, M. and Rundloef, H., *Ferroelectrics*, Vol. 261, pp. 193–198 (2001).
73) Corker, D. L., Glazer, A. M., Dec, J., Roleder, K. and Whatmore, W., *Acta Crystallogr. Sect. B: Struct. Crystallogr. Crys. Chem.*, Vol. B53, pp. 135–142 (1997).
74) Corker, D. L. Glazer, A. M., Whatmore, R. W., Stallard, A. and Fauth, F., *J. Phys.: Condens. Matter*, Vol. 10, pp. 6251–6269 (1998).
75) Noheda, B., Cox, D. E., Shirane, G., Guo, R., Jones, B. and Cross, L. E., *Phys. Rev. B*, Vol. 63, pp. 014103/1–014103/9 (2001).
76) Araujo, E. B., Yukimitu, K., Moraes, J. C. S., Pelaio, L. H. Z. and Eiras, J. A., *J. Phys.: Condens. Matter*, Vol. 14, pp. 5195–5199 (2002).
77) Bouzid, A., Bourim, E. M., Gabbay, M. and Fantozzi, G., *J. Eur. Ceram. Soc.*, Vol. 25, pp. 3213–3221 (2005).
78) Sawagushi, E., *J. Phys. Soc. Jpn.*, Vol. 8, pp. 615–629 (1953).
79) Leontev, N. G., Smotrakpv, V. G. and Fesenko, E. G., *Izv. Akad. Nauk SSSR, Neorg. Mater.*, Vol. 18, No. 3, pp. 449–453 (1982); *Inorg. Mater.* (Engl. Transl.), Vol. 18, No. 3, pp. 374–378 (1982).
80) Fesenko, E. G., Eremkin, V. V. and Smotrakov, V. G., *Fiz. Tverd. Tela*, Vol. 28, No. 1, pp. 324–326 (1986); Sov. *Phys.-Solid State* (Engl.Transl.), Vol. 28, No. 1, pp. 181–182 (1986).
81) Eremkin, V. V., Smotrakov, V. G. and Fesenko, E. G., *Fiz. Tverd. Tela*, Vol. 31, No. 6, pp. 156–161 (1989); *Sov. Phys.-Solid State* (Engl.Transl.), Vol. 31, No. 6, pp. 1002–1005 (1989).
82) Viehland, D., *Phys. Rev. B-Condens. Matter*, Vol. 52, No. 2, pp. 778–791 (1995).
83) Mishra, S. K. and Pandey, D., *Phylos. Mad.*, Vol. 76, No. 2, pp. 227–240 (1997).
84) Risold, D., Nagata, I. J. and Suzuki, O. R., *J. Phase Equil.*, Vol. 19, pp. 213–233 (1998).
85) Wang, C., Ph. D. Thesis, "Experimental and Computational Phase Studies of the ZrO_2 Based Systems for Thermal Barrier Coating," University of Stuttgart (2006).
86) Čančarević, M., Zinkevich, M. and Aldinger, F., Thermodynamic Reassessment of the Ti–O System, submitted to Calphad.
87) The SGTE substance database, version 1997, SGTE (Scientific Group Thermodata Europe), Grenoble, France (1997).
88) Muggiano, Y. M., Gambino, M. and Bros, J. P., *J. Chem. Phys.*, Vol. 72, No. 1, pp. 83–88 (1975).
89) Matsko, Y. and Sasaki, H., *J. Am. Ceram. Soc.*, Vol. 46, No. 8, pp. 409–410 (1963).
90) Ikeda, T., Okano, T. and Watanabe, M., *Jpn. J. Appl. Phys.*, Vol. 1, pp. 218–222 (1962).
91) Bannister, M. J., *J. Am. Ceram. Soc.*, Vol. 69, No. 11, pp. C269–C271 (1986).